SANDIA REPORT

SAND2016-2794
Unlimited Release
Printed March 2016

Characterization of Reconsolidated Crushed Salt from the BAMBUS Site

F. D. Hansen

Prepared by
Sandia National Laboratories
Albuquerque, New Mexico 87185-0751

Sandia National Laboratories is a multi-program laboratory managed and operated by Sandia Corporation, a wholly owned subsidiary of Lockheed Martin Corporation, for the U.S. Department of Energy's National Nuclear Security Administration under contract DE-AC04-94AL85000.

Sandia National Laboratories

Issued by Sandia National Laboratories, operated for the United States Department of Energy by Sandia Corporation.

Available to DOE and DOE contractors from
U.S. Department of Energy
Office of Scientific and Technical Information
P.O. Box 62
Oak Ridge, TN 37831

Telephone: (865) 576-8401
Facsimile: (865) 576-5728
E-Mail: reports@adonis.osti.gov
Online ordering: http://www.osti.gov/bridge

Available to the public from
U.S. Department of Commerce
National Technical Information Service
5285 Port Royal Rd.
Springfield, VA 22161

Telephone: (800) 553-6847
Facsimile: (703) 605-6900
E-Mail: orders@ntis.fedworld.gov
Online order: http://www.ntis.gov/help/ordermethods.asp?loc=7-4-0#online

SAND2016-2794
Unlimited Release
Printed March 2016

ABSTRACT

Observational petrofabrics, thermal, mechanical, and hydrological measurements were made on reconsolidated salt samples extracted from the field site in which a study called Backfilling and Sealing of Underground Repositories for Radioactive Waste in Salt was conducted. Similar characterization was completed more than a decade ago, so this work furthers previous measurements after sustained consolidation *in situ*. Porosity determined by traditional point-counting on polished sections and helium porosimeter methods ranged from 20-25% with consolidation governed by brittle processes, as evidence of fluid-aided, grain-boundary processes was rarely observed. Thermal conductivity in the range of 2.3 W/(m·K) is consistent for granular halite in this porosity range. Gas flow measurements yielded permeability of the order of $5e^{-13}m^2$. Pressure-sensitive compressive strengths at 0.5, 1.0, and 2.0 MPa confining pressure were 8, 9, and 14 MPa, respectively, with apparent elastic moduli increase with deformation.

ACKNOWLEDGMENTS

Mechanical strength and flow testing was performed primarily by Perry Barrow and data analyzed by Stephen J. Bauer and Scott Broome, all of the Geomechanics Department of Sandia National Laboratories. We are indebted to these professionals.

The Principal Investigator (Hansen) is collaborating in a mentoring capacity with graduate students Melissa M. Mills and Laxmi Paneru under the supervision of Professor John C. Stormont at the University of New Mexico. Methods and techniques used to measure characteristics of reconsolidated salt cores from the BAMBUS (Backfilling and Sealing of Underground Repositories for Radioactive Waste in Salt) site are directly related to their ongoing research interests. Interpretation of microstructures, porosity, density, permeability and other properties will enhance their thesis database, while providing high-quality results for our international collaborators. The equipment and techniques noted are being employed in their respective research.

The scientific measurements for this study were executed to requirements of the Waste Isolation Pilot Plant Quality Assurance program. Shelly Nielsen was instrumental in guiding the team through the rigors of training, qualifications, and obligations of the Quality Assurance procedures. This manuscript was professionally prepared by Laura A. Connolly. The cooperation and can-do attitude exhibited by these exemplary colleagues are gratefully acknowledged.

This work would not be possible were it not for long-term professional relationships with several scientists at the IfG (Institut für Gebirgsmechanik GmbH Leipzig Germany). The current investigations were facilitated by Peter Kamlot and Till Popp of IfG.

CONTENTS

FIGURES

TABLES

ABBREVIATIONS, ACRONYMS AND INITIALISMS

BAMBUS	Backfilling and Sealing of Underground Repositories for Radioactive Waste in Salt
BfS	Bundesamt für Strahlenschutz (Federal Office of Radiation Protection)
IfG	Institut für Gebirgsmechanik GmbH (Leipzig, Germany)
SEM	Scanning Electron Microscope
SNL	Sandia National Laboratories
UNM	University of New Mexico
WIPP	Waste Isolation Pilot Plant

1 INTRODUCTION

Reconsolidation of granular salt is an important consideration in current and future salt repositories for hazardous wastes, including nuclear. Processes by which crushed or granular salt reconstitutes itself into a solid material exhibiting properties of native salt are keys to understanding properties attributable at various stages of reconsolidation. This short report characterizes samples of reconsolidated salt recently extracted from a former Thermal Simulation of Drift Storage test site at the Asse Mine in Germany. Similar samples were recovered previously for the well-known BAMBUS (Backfilling and Sealing of Underground Repositories for Radioactive Waste in Salt) research and forensic studies (Bechthold et al. 2004). Measurements are explained in sufficient detail that they could be repeated independently by peers with equal expertise. Several of the techniques employed were reported previously (Bechthold et al. 2004). The crushed salt backfill associated with the BAMBUS forensic work reported earlier has now experienced another decade of consolidation in the underground setting. Collaborators in international salt repository investigations have agreed another series of characterization studies on the BAMBUS reconsolidated salt would help elucidate large-scale, long-term consolidation processes.

Because of a long-term professional and scientific relationship between Sandia National Laboratories (SNL) and the Institut für Gebirgsmechanik GmbH (Leipzig, Germany) (IfG), an opportunity arose to obtain and to examine additional core material from the BAMBUS site. Within the scope of the Asse geomechanical assessment of the operational phase, IfG acquired new borehole core from the BAMBUS site, as documented in Appendix A. The aim is to characterize the compacted crushed salt material again in order to obtain a further reliable reference point for the calibration of the modeling approaches to be used. After approval by Bundesamt für Strahlenschutz (Federal Office of Radiation Protection-BfS), residual sample material is being used to examine and measure current characteristics of the backfill, make assessments of its properties, and describe reconsolidation processes and mechanisms. Four relatively small cores were obtained during a site visit to IfG in connection with an independent project meeting.

Crushed salt reconsolidation is a contemporary issue for the Waste Isolation Pilot Plant (WIPP) because of a recent change of panel closure design to one which comprises principally run-of-mine crushed salt. As this line of research continues, findings will pertain to design, analysis, operations and performance of any other salt repository in which crushed or run-of-mine salt plays a role in isolation systems. Salt as a geologic medium has several attributes favorable to long-term isolation of material placed in mined openings. Salt formations are largely impermeable and induced fractures heal. Permanent isolation also depends on the ability to construct geotechnical barriers that achieve high-performance characteristics attributed to the native salt formation. Lingering uncertainty with geotechnical barriers constructed of granular salt pertains mostly to the limits involved with testing over extended time periods and at an appropriately large scale+. To strengthen the technical basis for salt-seal systems, natural and anthropogenic analogues can be used to exemplify cases where salt reconstitutes itself into an impermeable medium. Invoking analogue examples provides an independent line of reasoning to safety case performance arguments. Therefore, these forensic studies of the reconsolidated BAMBUS salt add to the analogue database as well as provide pertinent information for technical assessments being made by our German colleagues.

In previous cooperation with international colleagues, the Carlsbad Field Office advanced scientific knowledge of salt properties pertinent to WIPP through Work Packages undertaken by BAMBUS collaborators. Overall the experiment itself and the post-test forensics comprise many elements of direct relevance to WIPP operations and its performance assessment as well as salt repository future activities. Sandia's previous investigations associated with BAMBUS focused on crushed salt reconsolidation and the excavation disturbed zone. Current studies characterize basic properties and characteristics of reconsolidated crushed salt backfill from the BAMBUS setting.

1.1 Equipment

The author of this report is also collaborating with the University of New Mexico (UNM) on a research project sponsored by Nuclear Engineering University Partnerships: *Improving the understanding of the coupled thermal-mechanical-hydrologic behavior of consolidating granular salt.* The UNM research is examining granular salt consolidation through an integrated program of laboratory measurements, observations, and model development. UNM researchers have been taught specimen preparation techniques, measurement methods, and received hands-on observational instruction and interpretation in pursuit of their various thesis objectives. The BAMBUS core provides a real-life example that can be compared to their measurements on laboratory samples. The students will apply their techniques and make measurements on BAMBUS core samples using experimental processes embodied in their thesis research.

Microstructural observations are made with optical and electron beam microscopes. There are many optical and scanning electron microscopes (SEM) that would provide equally sufficient images. Characterization of the BAMBUS cores is directly related to their ongoing research interests. Interpretation of microstructures, porosity, density, permeability and other characteristics provides high-quality results for our international collaborators. Below are descriptions of equipment and techniques applied, such that any other equally trained person can replicate this work. However, reference to specific commercial equipment does not constitute or imply endorsement. Other instruments with similar capabilities could be used.

1.1.1 Optical Microscope

A Leitz Ortholux II optical microscope, Figure 1.1, uses combined transmitted and incident polarized light with a five objective nosepiece to examine samples. The microscope is equipped with a Leica camera and Leica Application Suite software to capture images. The optical scope was used for point-counting porosity and petrophysical descriptions. Much of the microscopic documentation is captured by photography.

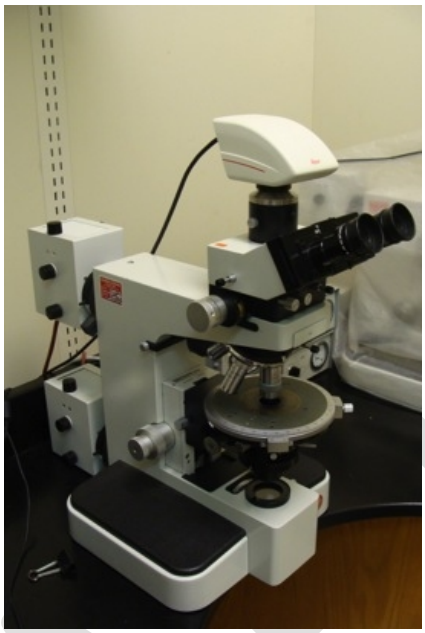

Figure 1.1. Leitz Ortholux II optical microscope.

1.1.2 Stereo Inspection Microscope

A Lynx eyepiece-less stereo inspection microscope, Figure 1.2, with dynascope technology is used to look at larger (hand-held) samples. The optics allow for a large viewing area with a 3-dimensional, high-resolution image. The range of stereo zoom magnification is 3.5x to 120x provided by the step magnification multiplier.

Figure 1.2. Lynx stereo inspection microscope.

1.1.3 Scanning Electron Microscope

The JEOL 5800LV SEM, Figure 1.3, uses a beam of electrons to scan a sample in order to create surface images at high magnification (up to 300,000X). The JEOL is equipped with secondary and backscattered electron imaging detectors as well as a cathodoluminscence imaging detector.

The instrument uses the Oxford Isis 300 analytical system, which includes an energy dispersive X-Ray spectroscopy detector, to acquire sample images and composition.

Figure 1.3. JEOL 5800LV scanning electron microscope.

An FEI Nova 200 Nanolab, Figure 1.4, is an instrument with a dual beam system of a focused ion beam column and SEM column. The SEM column is equipped with a tungsten filament for imaging in low or high vacuum levels. The detector has a resolution of 3.5 nm operating at 30 kV at high vacuum and less than 15 nm at 3 kV when operating in low vacuum. The instrument is also equipped with INCA Synergy 350 with HKL Premium EBSD System, which allows elemental analysis of samples as well as the capability of generating phase maps from elemental maps and Cameo data. An HKL Premium Electron Backscatter Detector can be used within the machine for crystallographic determination to create orientation maps of microstructures, generate combined orientation and elemental maps, and generate pole figures.

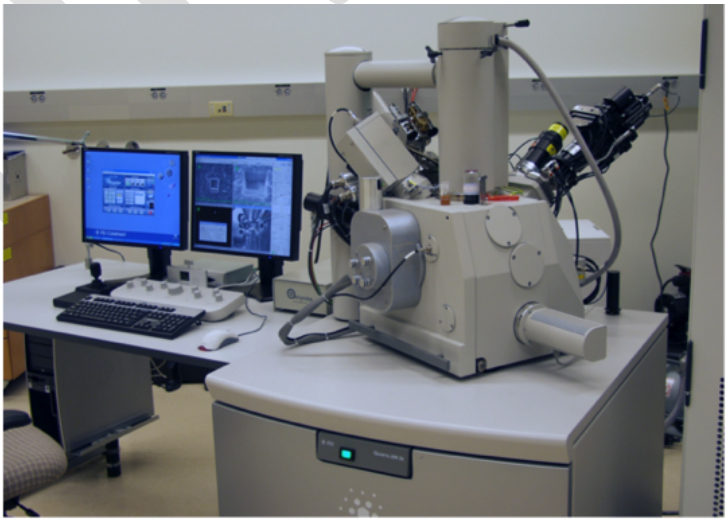

Figure 1.4. FEI Nova 200 Nanolab SEM.

1.1.4 Sputter Coater

To prepare non-conducting or poorly conducting samples for observation in an SEM, a sputter coater must be used. The EmiTech KX950 sputter coater, Figure 1.5 allows samples to be thinly

coated with carbon or gold-palladium to increase electrical conduction. This device is equipped with a turbo pump evaporator for complete automatic control during evaporation of the chamber to low pressures while having a dry gas inlet to improve coating deposition. This sputter coater is also used with a K150X film thickness monitor that measures the thickness of the coating that has been deposited on a crystal within the chamber.

Samples can be coated with carbon or gold-palladium. A carbon rod with a 3mm sharpened spigot shaped head is ignited and evaporated producing a 25nm thick coat for a 5 second pulse. Carbon coating is generally used for mass samples and gold-palladium is used etched surfaces to obtain high-resolution coating. It is a constant challenge to produce an optimal thickness. From experience, a 9.5nm thickness produces the best results.

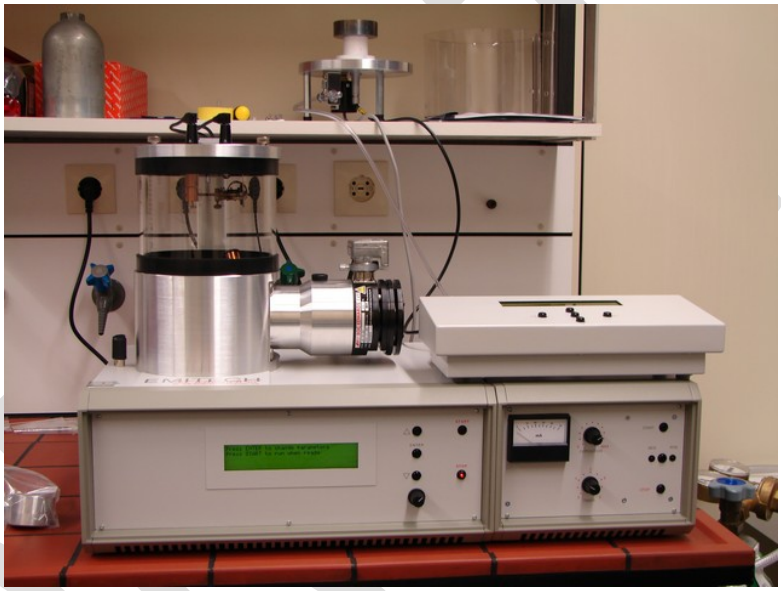

Figure 1.5. EmiTech KX950 sputter coater with K150X film thickness monitor.

1.1.5 Diamond Wire Saw

The BAMBUS core samples needed to be cut and prepared in special ways to make thin-sections, create fragments, prepare thermal conductivity and permeability/strength cylinders. A diamond wire saw, shown in Figure 1.6, was used to prepare subsamples. Samples of interest are clamped in place on the platform to ensure they do not move while cutting. The saw mechanism changes rotating directions using magnetic sensors, which allows the wire to be pulled back and forth. A small amount of weight (about 5 grams) on the wire arm slowly lowers the wire through the sample. Sensors located on the sides of the arm control the stroke and shut-off.

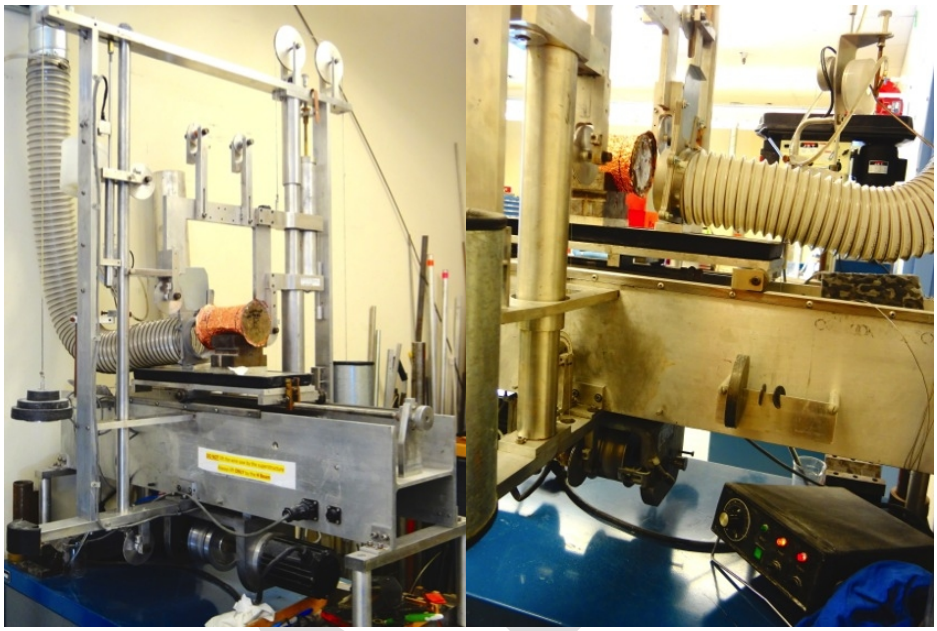

Figure 1.6. Diamond wire saw with ventilation, pulley system, adjustable table, wheel, pump and pump controller.

1.1.6 IsoMet Low Speed Saw

A Buehler IsoMet low speed saw, shown in Figure 1.7, is used for making precision cut thin sections with a diamond-impregnated blade. A specimen of interest is glued to a glass slide, which is suctioned onto vacuum chuck holder. The holder is then screwed onto the arm above the blade and its position adjusted by a micrometer. The micrometer allows for manual determination of thickness for each cut. Weights on the arm control the loading of the specimen, which governs the speed of the cut. For salt specimens, isopropanol is used as the cutting liquid and is poured into a reservoir below the blade, refilling regularly due to evaporation.

Figure 1.7. Buehler IsoMet low speed saw.

Sample material is impregnated with epoxy as described subsequently. Excess epoxy can be cut away with a knife, band saw, or other convenient method. Impregnated samples are then cut to size for a petrographic slide. Thin sections for optical petrography are challenging to make because they are extremely thin—having an optical path difference between 530 and 560 nanometers. Fortunately, much of the information of interest can be obtained from thick-thin sections (~3 mm thick). Optical microscopy is used for observations of deformation processes, grain boundary conditions, void spaces, fabric, mineralogy and any other notable characteristics. Petrographic sections can also be etched and examined optically or by SEM.

1.1.7 Ecomet III Polisher and Grinder

Figure 1.8 shows a Buehler Ecomet III polisher and grinder, which is used to polish petrographic sections after cutting and also to create smooth, even surfaces on other types of samples. Abrasive, circular paper, ranging in grit size from 400 to 1200, is adhered to a rotating wheel. The paper is wetted with isopropanol and samples are held on the wheel with minimal pressure until a smooth surface is obtained.

Figure 1.8. Buehler Ecomet III polisher and grinder.

1.2 Sample Preparation

1.2.1 Impregnation

Typically, the solid state of the sample is locked in place by impregnation with low viscosity epoxy. Samples are shaped to a convenient size for thin- or thick-section preparation using the slow-speed, low damage wire saw. There are many types of epoxy that can be used. We use a two-component epoxy which is stained blue and has performed well in similar sample preparation (RF 1366 commercially available epoxy from Resin Formulators). The sub-sample is placed in a convenient disposable container (a paper cup or aluminum foil, for example). The sample is completely immersed in epoxy and placed in a bell jar, which is put under approximately 10 psi vacuum (approximately 3 psia inside the bell jar). After the system has been evacuated, the vacuum is removed slowly by venting and atmospheric pressure helps force

epoxy into the evacuated voids of the specimen. This process is repeated 3-4 times to ensure that the specimen has been fully impregnated. The epoxy is then allowed to cure.

1.2.2 Polishing

Cutting with the diamond-wire saw creates a relatively smooth surface with small ridges. To improve imaging on the stereo-dynascopic or optical microscopes, uneven surfaces need to be smoothed by polishing, which is done using a clean, flat surface, a sheet of sandpaper, and isopropanol. For salt, 400 to 600 silicon carbide sand paper has been shown to produce an acceptable surface. Isopropanol is used as the wetting agent and a figure-eight motion seems to create a nice finish.

1.2.3 Etching

Salt can be etched by agitating in a solution of methanol saturated with $PbCl_2$ and stopped with butanol. Etching requires practice. Typically, a single chip is held with a tweezers and agitated in the $PbCl_2$ solution for 3 to 4 seconds and stopped immediately by transfer to butanol. Excess liquid can be drawn off by dropping the chip on a dry Kimwipe®. Etching highlights the substructure in the crystal lattice, which can be immediately examined on an optical scope. This quick examination also allows evaluation of how well etching was done. Crisp etches with sharp contrast and resolution facilitate evaluation of the substructure. After cleavage chips are successfully etched, they are mounted with carbon tape and coated in gold-palladium for observation under the SEM where high-magnification the etched surface is possible.

1.3 Samples from the BAMBUS Site

Locations within the underground setting from which cores were extracted are documented in Appendix A. Photographs of the cores selected are also shown in Appendix A. The core was packaged carefully and hand-carried from Germany to the USA. As will be shown in the photographic records, the as-obtained material ranged from competent to fragile.

Four samples were selected from the inventory available at IfG. Two samples from each borehole were selected. From borehole 1, samples at 1.82 m and 2.77 m depth and from borehole 2, a sample at 2.5 m and a small sample near the end of the borehole labeled “bis end” were selected. Each of these samples was used to create sub-samples for characterization, which exhausted the core available. Sub-sample identification and use are given in Table 1.1, with BH1 and BH2 denoting borehole 1 and borehole 2, respectively. The depth of the sub-sample is included in its identification. Further division of samples are simply denoted A, B or Center. Typically the A and B sub-samples would be end pieces, with the center representing the longest piece available for permeability and deformation testing. For example, BH2-2.5m-B-1 is one of the end pieces from a sample from borehole 2 at 2.5m depth, which has been sub-divided for specific sample preparation.

Table 1.1. Sample identification and usage

Sample Original ID	Sub-sample	Use
KBrg-1(1.82 m)	BH1-1.82m-A	Thermal/Porosity
	BH1-1.82m-B	SEM/Optical Microscope
	BH1-1.82m-Center	Permeability/Strength
KBrg-1(2.77 m)	BH1-2.77m-A	Thermal/Porosity
	BH1-2.77m-B	SEM/Optical Microscope
	BH1-2.77m-Center	Permeability/Strength
KBrg-2(2.5m)	BH2-2.5m-A	Thermal/Porosity
	BH2-2.5m-B-1	SEM/Optical Microscope
	BH2-2.5m-B-2	
	BH2-2.5m-Center	Permeability/Strength
KBrg-2 (bis end)	BH2-HD-A	Thin Sections
	BH2-HD-B	SEM/Optical Microscope

2 CHARACTERIZATION

Characterization included qualitative descriptions as well as quantitative test measurements.

2.1 Scanning Electron Microscopy

Fragments can be obtained several ways. Part of observational studies of reconsolidated salt involves use of a "fresh face" that has not been cut or polished. Usually fragments from cut ends can simply be broken by flexure. This exposes a clean surface, which exhibits diagnostics of sample cohesiveness, grain boundary characteristics, and other evidence of microprocesses. The SEM is convenient for these observations because of its focal length. Fragments provide a sense of 3-D imaging, particularly useful for examining grain boundaries.

Scanning electron microscopy of fragments allows close examination of grain-to-grain interaction, a general 3-dimensional appreciation of the void space, and characteristics of consolidation processes. Eight images are shown in Figure 2.1 and labeled A-H. There are four micrographs for each borehole. Five images are shot at 350X magnification (~250 μm across the field of view) and the remaining three are at higher magnification to examine a few fine features of interest. A scale bar appears on each image.

Four representative images are provided from each borehole. We did not attempt to provide equal or statistical sampling, but rather to capture representative physical processes.

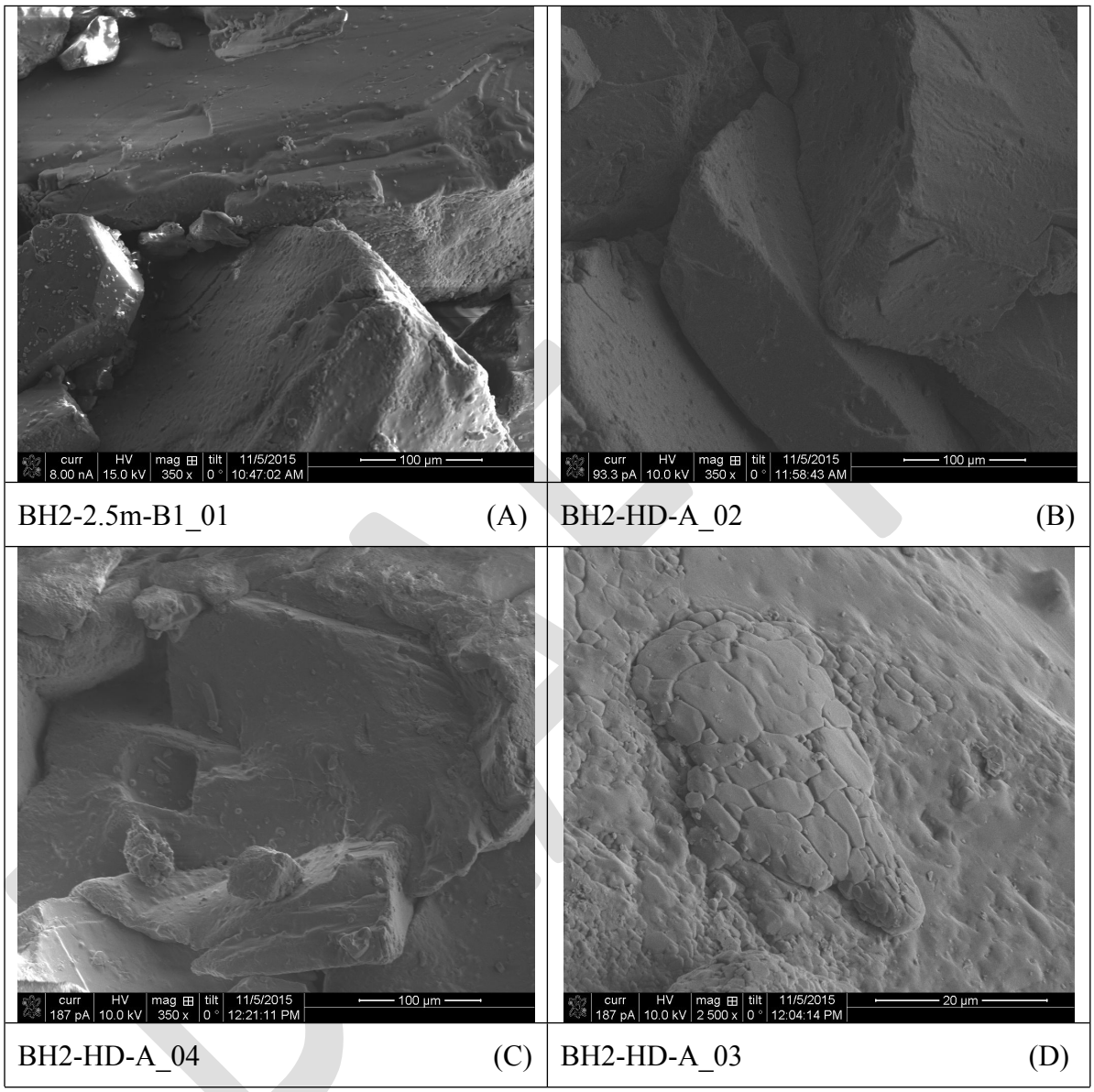

BH2-2.5m-B1_01	(A)	BH2-HD-A_02	(B)
BH2-HD-A_04	(C)	BH2-HD-A_03	(D)

Figure 2.1. Scanning electron images of BAMBUS salt.
(Part 1)

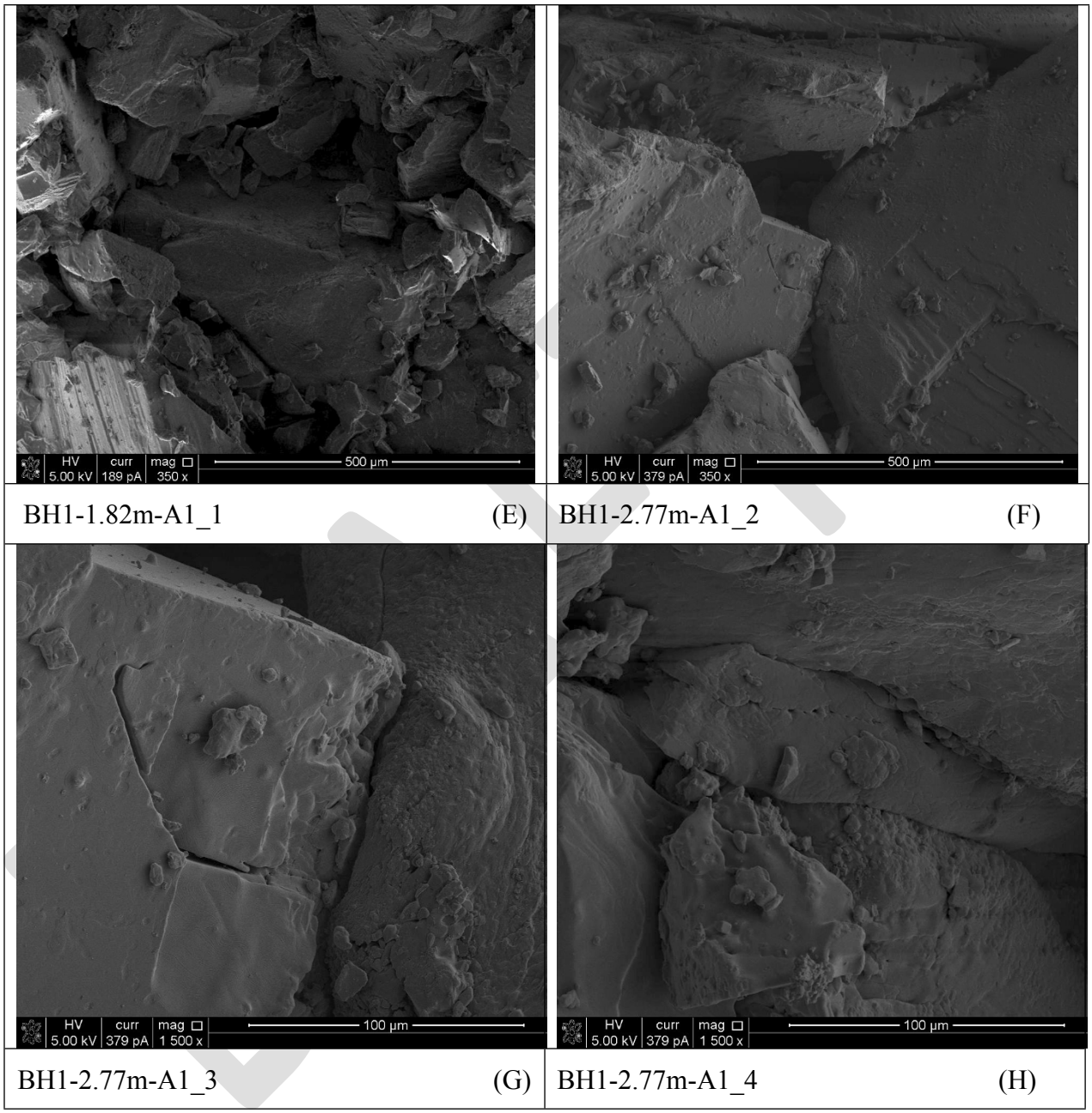

Figure 2.1. Scanning electron images of BAMBUS salt. (Part 2)

A, B, and C are shot at 350X magnification and illustrate angular voids preserved between grain contacts. Abrasion roughens grain surfaces and is seen on most grain boundaries. The compacted mass has established relatively tight grain boundaries created by translational sliding, as exhibited in micrograph **B**. Local crystal plasticity can be seen in micrograph **C**. No suturing by fluid assisted processes is evident at 350X; however, micrograph **D** at 2500X captures a small-scale cohesion mass of fine grains within a boundary looking approximately normal to the plane.

Micrograph **E** is an example of a fragile fragment face with notably higher porosity and loose aggregate. Micrograph **F** is comparable to **A** in terms of porosity and void architecture, but also

captures images of plasticity and incipient fracture at the grain contact near the center of the frame. This image is enhanced in micrograph **G**, where fracture is developing in the left grain and plastic ridges are piling up on the right grains. Micrograph **H** illustrates tight compaction with gouge along the upper boundary of the elongate grain in the center of the field of view. Again, there is minimal evidence for fluid-aided grain-boundary processes. The level of consolidation by mostly brittle translational compaction varies considerably as will be reflected subsequently in porosity measurements.

2.2 Thermal Conductivity and Porosity Measurements

Thermal conductivity was measured on two samples from borehole 1 and one sample from borehole two, as delineated in Table 1.1. After thermal conductivity was measured, small cores were extracted for porosity measurements. Additional porosity measurements were also made by standard point-counting techniques. This section describes how these measurements were made and results obtained. The reconsolidating salt from the BAMBUS site has a degree of variability, which these measurements tend to bracket. Thermal properties vary with porosity, so we measured porosity and thermal conductivity on the same samples, if possible.

Two nearly identical pieces were cut from the core using the diamond-wire saw. Each piece was polished on one side using fine sand paper and isopropanol to create a smooth surface. This operation cleaned salt dust and removed asperities from the surface. After polishing, a Kapton® thermal sensor was pressed between the two pieces. One of the pieces was placed on the mounting table of the sample holder and its height adjusted so that the surface of the sample was the same level as the sensor. The second sample disc was placed on the sensor and mounting pressure was applied using a screw. A heat pulse of 400 mW was supplied by the Thermal Constants Analyzer to the sample pieces and thermal properties were measured in 40 seconds. Heat energy was dissipated by waiting 20 minutes between runs. Typically, three to five measurements at each temperature were made and averaged. In terms of data quality objectives, standard deviation may range between 10^{-2} to 10^{-3} W/(mK).

After thermal properties were measured, porosity measurements were obtained on the same material. The thermal conductivity sample was cored to obtain a 1-inch or 1.5-inch-diameter circular disk. The choice of diameter was a judgment call depending on the degree of consolidation or cohesiveness. The cored sample was then cut on the diamond wire saw to a height of 0.5 inches and polished to obtain a uniform geometry. Typical test specimens are shown in Figure 2.2.

Figure 2.2. Samples for porosity measurements.

A helium gas expansion porosimeter is used to determine effective porosity (see Figure 2.3). It is based on Boyle's law of gas expansion. The apparatus consists of a reference volume and a sample cell volume, separated on either side by a valve V_2 as shown in Figure 2.4. Before the actual porosity measurement is conducted, the sample cell of the porosimeter is calibrated under two different conditions: sample cell with all the billets inside and sample cell without a 0.5-inch thick billet. The cored sample disc is put in the sample cell to replace a billet of an equivalent diameter and volume. The external valve V_3 on the right is left open to the atmosphere and central valve V_2 is closed. The reference section is filled through the left valve V_1 with helium at a load pressure of P_o= 100 psi. After the reference section is shut in from main gas supply and pressure Po is recorded, the sample section is shut by closing the valve to the atmosphere. After this, the central valve V_2 is opened to allow the gas in the reference section to pass into the sample section. The pressure is allowed to equilibrate for 15 seconds, and the equilibrium pressure P is recorded for at least three measurements and averaged. This practice follows helium gas expansion porosimeter user's manual provided by Frank Jones and Associates, Inc.

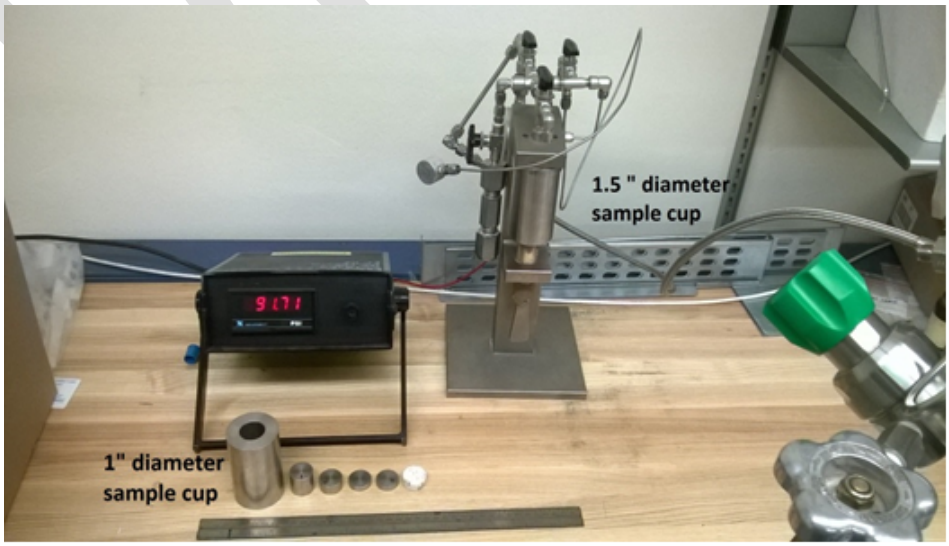

Figure 2.3. Porosimeter test set up.

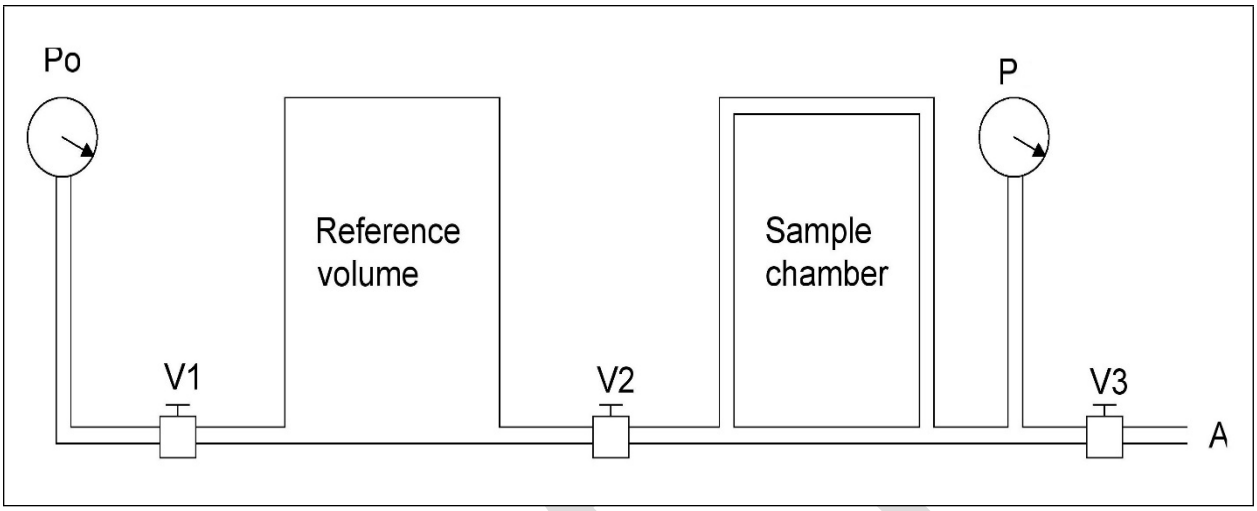

Figure 2.4. Schematic of porosimeter method.

The grain volume is given by,

$$G=B+\frac{Pof}{Pf}R-\frac{Pos}{Ps}R$$

where, P_{os}, P_s= initial and final pressures during a porosity test, when a 1" or 0.5" billet is replaced by an equivalent volume of sample.

The reservoir volume is given by,

$$R=\frac{B}{\frac{Pob}{Pb}-\frac{Pof}{Pf}}$$

where, B=volume of the removed 1" or 0.5" billet.

P_{ob}, P_b= initial and final pressures during calibration of the cell, when a 1" or 0.5" billet is removed.

P_{of}, P_f= initial and final pressures during calibration of the cell, when all the billets are inside the cell.

Measurement of diameter and height is carried out at a number of locations on the sample using calipers. Volume is calculated from dimension averages and bulk density is calculated from mass and volume. Grain density is calculated from the grain volume and mass.

Porosity φ is calculated by

$$\varphi = 1- B_D/G_D$$

where, B_D= bulk density (g/cc) and G_D= grain density (g/cc).

Another method called the small volume method, determines the total porosity of the sample. The sample core used in the porosimeter method is also used in this method. Bulk density is calculated from measured mass and volume. Grain density is assumed as 2.16 g/cc.

Porosity and thermal properties determined in tandem are presented in Figure 2.4 and Figure 2.5. Both boreholes were sampled and measured. Borehole 1 at 1.82 has the highest porosity, ranging around 24%. Compare to photomicrograph **E** of Figure 2.1. Borehole 1 at 2.77 m reflects the lowest porosity of samples measured, around 20%. The SEM photomicrographs **F**, **G**, and **H** capture grain arrangement and pore space of this lower porosity. It is clear that porosity and thermal properties vary throughout, but measurements provide a reasonable range.

1. Porosity of BAMBUS salt by porosimeter and small volume methods.

Sample ID	Porosimeter (%)				Small volume (%)			
	Core 1	Core 2	Core 3	Avg ϕ	Core 1	Core 2	Core 3	Avg ϕ
BAMBUS-1-1.82	25.31	24.62		24.97	23.52	23.75		23.64
BAMBUS-1-2.77	22.04	20.31	20.35	20.90	21.39	19.49	19.49	20.12
BAMBUS-2	26.17			26.17	25.09			25.09

2. Porosity vs thermal conductivity

Sample	Porosity		Thermal conductivity (50˚C)
	Porosimeter	Small volume	
BAMBUS-1-1.82	24.97	23.64	2.15
BAMBUS-1-2.77	20.90	20.12	2.48
BAMBUS-2	26.17	25.09	2.20

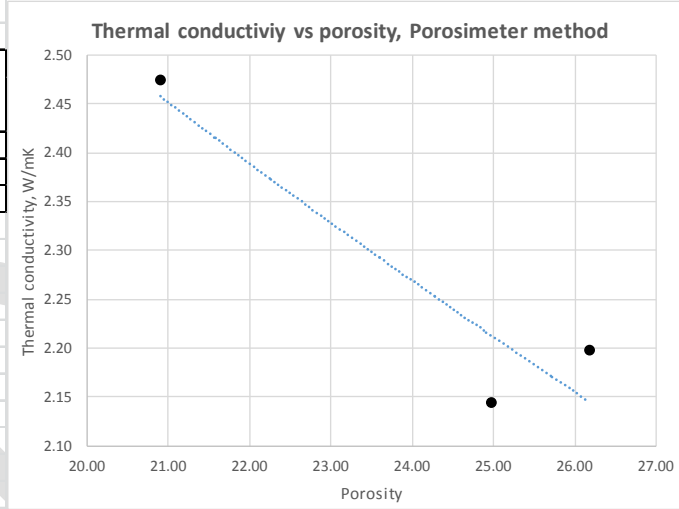

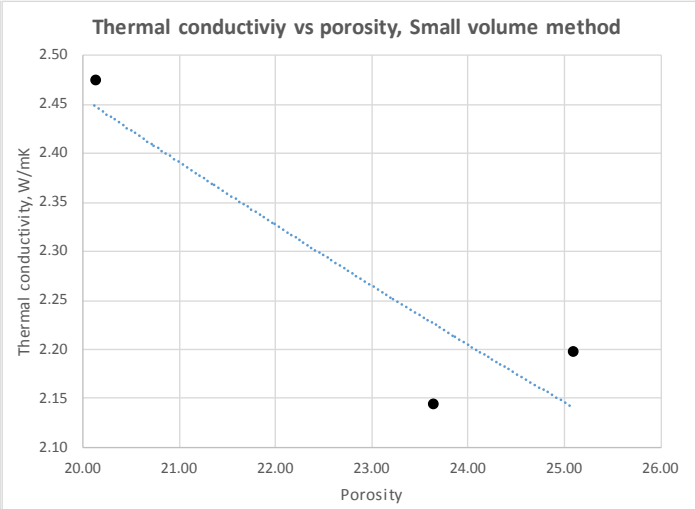

Figure 2.4. Porosity and thermal conductivity.

Sample ID	Temperature (˚C)	Avg. thermal conductivity (W/mK)	Avg. Thermal diffusivity (mm^2/s)	Avg. specific heat (MJ/m^3k)
BAMBUS-1-1.82	50	2.145	1.684	1.273
BAMBUS-1-1.82	100	1.971	1.385	1.424
BAMBUS-1-1.82	150	1.611	1.337	1.372
BAMBUS-1-2.77	50	2.475	1.754	1.413
BAMBUS-1-2.77	100	2.25	1.472	1.528
BAMBUS-1-2.77	150	1.832	1.261	1.453
BAMBUS-02	50	2.198	2.079	1.06
BAMBUS-02	100	2.013	1.58	1.273
BAMBUS-02	150	1.68	1.353	1.255

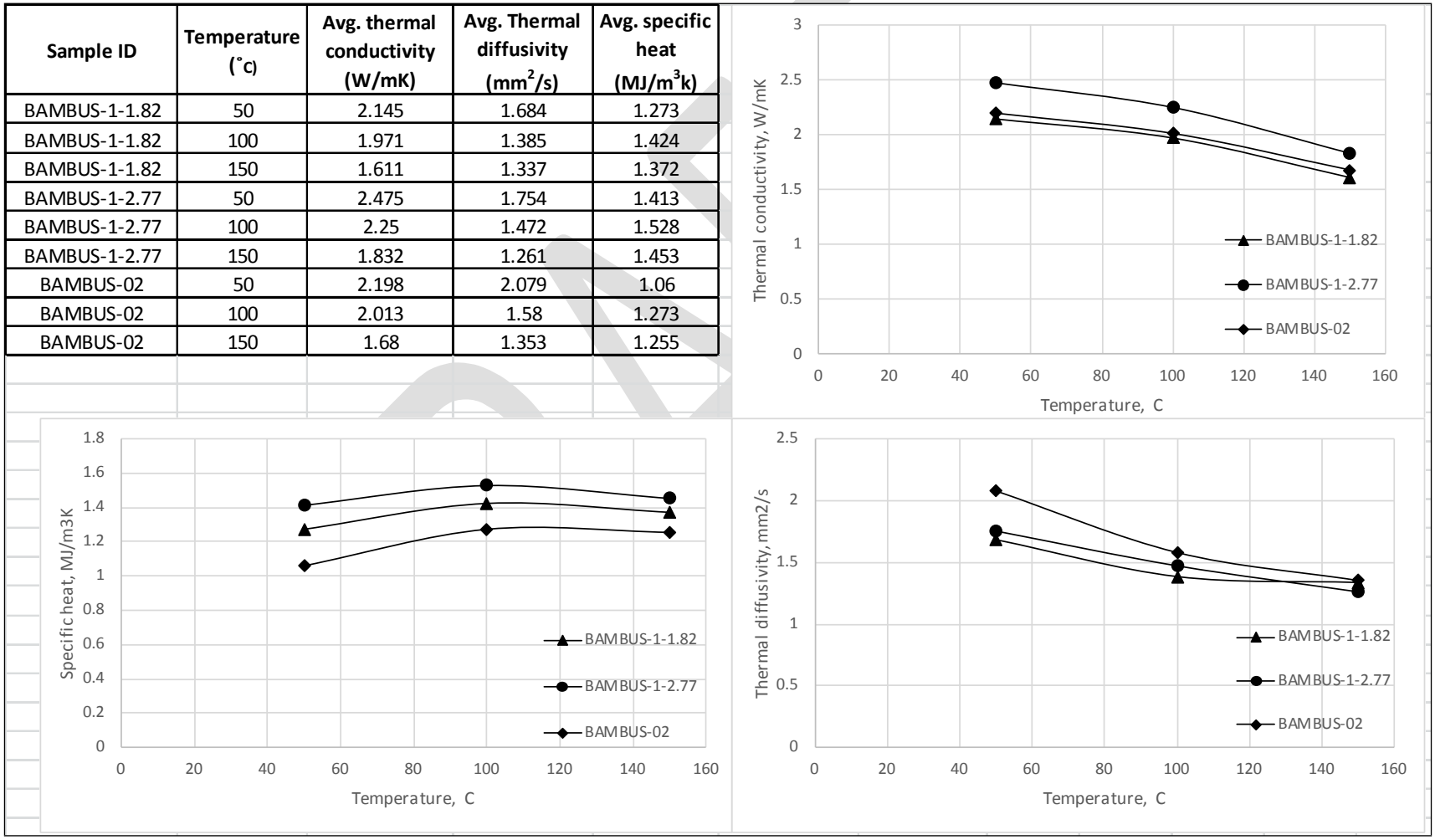

Figure 2.5. Thermal properties of BAMBUS reconsolidated salt.

We made a series of optical slides referred to as *thick-thin* sections. This oxymoronic nomenclature differentiates salt sections prepared at a thickness of 5 mm from typical rock petrographic sections that are 30 µm thick. These sections all derive from the small (bis end) piece from borehole 2 identified as BH2-HD-A (See Table 1.1). The thick-thin sections are identified in Table 2.1. An optical image of one of these thick-thin sections is shown in Figure 2.6. Slides such as shown in Figure 2.6 were used to systematically point count solid grains and void space. Porosities measured are in general agreement and compare globally to values determined by other methods. As a matter of accuracy and data quality, we performed independent measurements on the same sections and the results are summarized in Table 2.1. The results combine natural variability of porosity and interpretations of the operator. When independent operators counted the same slides (BH-D3 and BH-D4), average porosity was within 2%. It might be possible to reduce variance by substantially more point counting, but such measures have not been undertaken.

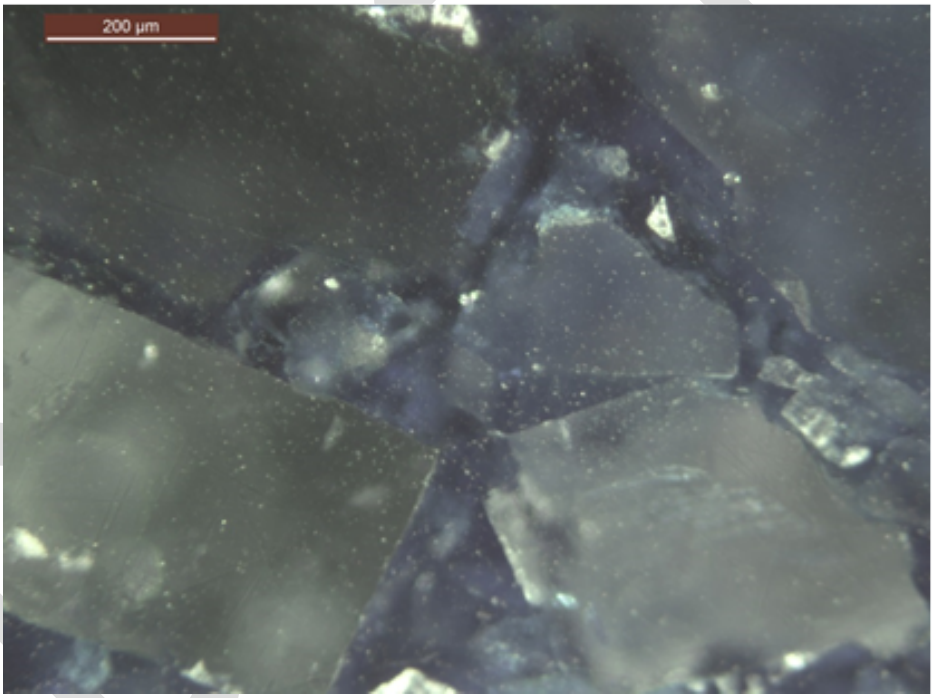

Figure 2.6. Typical thick-thin section of BAMBUS reconsolidated salt.

Table 2.1. Comparison of porosity determined by point counting

Thin Section Identification	Voids/Hansen %	Voids/Mills %
BH-D2	20.3	
BH-D3	25.0	30.7
BH-D4	28.3	26.7
BH-D5		28.3

3 GAS FLOW AND PERMEABILITY ESTIMATES

Gas flow measurements were completed on three samples and subsequently tested for strength.

3.1 Procedures

Test specimens were placed between two metal platens having central ports that permit the permeant (nitrogen) to enter and exit the specimen. Highly-permeable porous felt metal disks were placed in the interface between the platens and specimen to distribute the permeant and permeant pressure across the full cross-section of the specimen. Specimens were jacketed with painted-on polyurethane that seals by adhesion to the platens and salt core and serves to protect the specimen from hydraulic confining fluid and to prevent permeant from short-circuiting around the sides of the specimen during testing. A shrink tube was placed over the polyurethane, followed by an additional layer of painted-on polyurethane. Figure 3.1 shows an unjacketed sample, a jacketed sample before testing, and a jacketed sample after testing.

Figure 3.1. Unjacketed, jacketed pretest, and jacketed post test sample.

The jacketed specimen/platen assembly (Figure 3.2) was placed inside a pressure vessel and the upstream and downstream ports of the platens were connected to a permeant source and to a flow meter as part of the overall test system shown in Figure 3.3. The annulus between the specimen and pressure vessel was filled with Isopar® fluid and pressurized during the test (applying a pressure to the external surfaces of the specimen) to assure gas flowed through the sample and not between the jacket and sample by maintaining the confining pressure higher than the permeant pressure.

Figure 3.2. Jacketed sample with flow nipples.

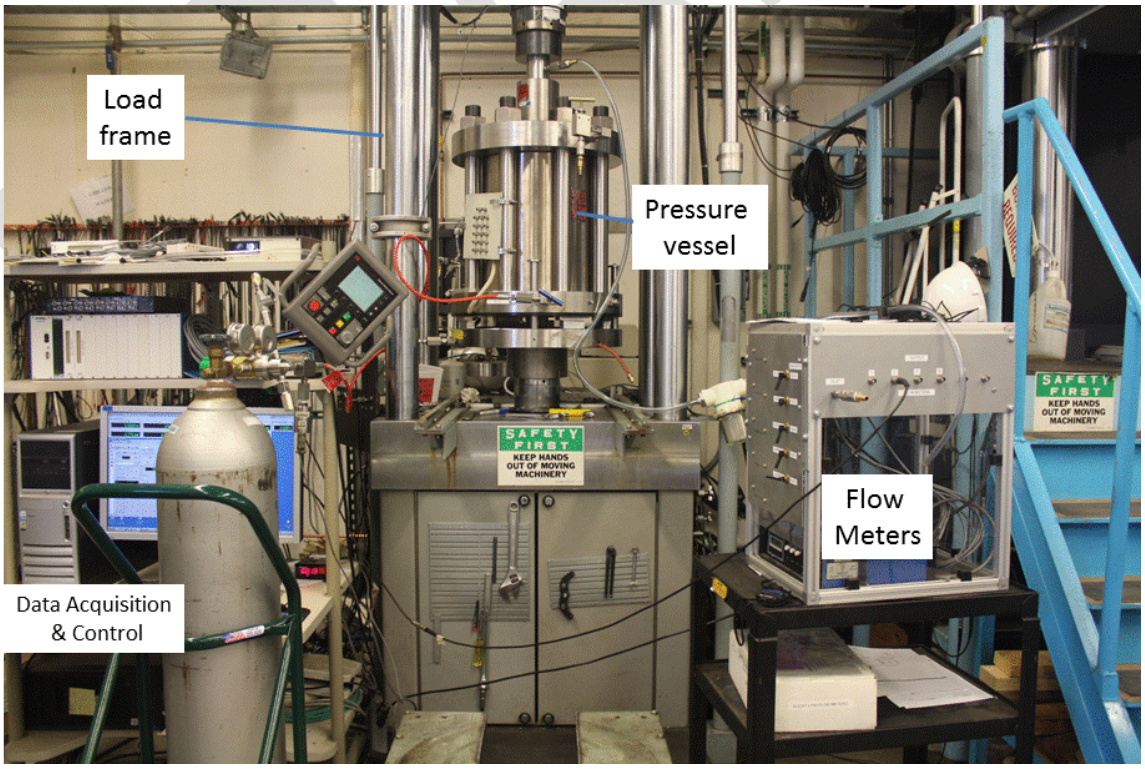

Figure 3.3. Testing system used to conduct gas flow and quasi-static triaxial compression tests.

The permeability measurement used a constant head (or pressure) technique with nitrogen as the permeant gas. In this technique, once the confining pressure has raised and stabilized to a constant value, permeant was allowed to enter the upstream side of the specimen at a constant

pressure (~0.036 MPa gage). The pressure difference between the upstream and downstream ends of the sample was minimized. The downstream side of the specimen was vented to the atmosphere through a flow meter. The flow meter was connected to the data acquisition system and presented flow in cc/min.

Test specimens were instrumented to measure axial displacements via Linear Variable Differential Transformers located in the actuator; thus, only axial displacements were measured during triaxial loading.

Figure 3.3 shows an example of the computer-controlled servo-hydraulic testing system used to conduct compression tests at ambient temperature. The system consists of an MTS® reaction load frame, coupled with a Structural Behavior Engineering Laboratory pressure vessel. The pressure vessel housing the test specimen was connected to a pressure intensifier to apply the confining pressure. Isopar® is used as the confining medium. The reaction frame has a movable crosshead to accommodate pressure vessels of different sizes and configurations. Vessel pressures were measured with a transducer located about 1.5m from the vessel plumbed directly into the tubing connecting the pressure vessel to the pressure intensifier. Axial forces were measured with a load cell attached to the reaction frame outside of the pressure vessel.

The setup and conduct of tests began by placing the jacketed and instrumented specimen onto the base of the pressure vessel, assembling the pressure vessel and placing it into the reaction frame. The actuator in the base of the frame was raised gradually to bring the pressure vessel piston into contact with the reaction frame. The pressure vessel was then connected to the pressure intensifier and filled with Isopar®. At this point the servohydraulic control was turned on and data collection began. The confining pressure was raised to the target confining pressure, with the reaction frame actuator holding its position. The test sequence followed the basic steps below:

1) A gas flow measurement was made.
2) Axial load was increased at a constant predetermined displacement rate (10^{-4} or 10^{-5} sec^{-1}). An axial load/unload cycle was performed at constant confining pressure so Young's Modulus could be determined. Two or more load/unload/reload loops were performed for each test.
3) The specimen was loaded to approximately 10% axial shortening.
4) In some cases, a post deformation flow test was performed.
5) Tests were ended by returning to a hydrostatic condition, followed by lowering confining pressure.

3.2 Results

Intrinsic permeability, k (in units of meters squared) was calculated from the following equation:

$$k = \frac{2\mu L Q_e P_{ea}}{A\left(P_{ia}^2 - P_{ea}^2\right)}$$

where:

μ is dynamic viscosity of the permeant (= 0.018×10^{-3} N· sec/m^2 for nitrogen)
L = specimen length (in meters)

A = specimen cross-sectional area (in meters squared)
Q_e = steady-state permeant flow rate (in cubic meters per second)
P_{ia} and P_{ea} are the inlet and exit absolute pressures (in Pascals)

Table 3.1 contains pertinent information appropriate for permeability estimation. Measurements were made at the test confining pressure for each sample. The confining pressure effect is expected to be small and insignificant.

Table 3.1. Sample designations, dimensions, density, estimated permeability

Sample ID	Diameter (in)	Diameter (cm)	Length (in)	Length (cm)	Mass (g)	Density (g/cc)	Confining Pressure (MPa)	Estimated Permeability (m2)
BH1-1.82m	3.273	8.31342	4.273	10.85342	976.2	1.66	0.5 pre deformation	5.8E-13
BH2-2.5m	3.944	10.01776	5.027	12.76858	1726.8	1.72	1.0 pre deformation	4.5E-13
							1.0 post deformation	3.2E-13
BH1-2.77m	3.277	8.32358	4.879	12.39266	1161.2	1.72	0.5 pre deformation	6.9E-13
							1.0 pre deformation	6.1E-13
							2.07 pre deformation	5.6E-13
							2.07 post deformation	5.8E-13

Axial stress versus axial strain plots for the three samples are given in Figure 3.4. Strength increased with increasing confining pressure. We note that these samples did not have the preferred 2:1 aspect ratio. Table 3.2 provides information of calculated moduli from the unload/reload loops during triaxial testing. Generally, modulus increased with increasing confining pressure as well as increasing axial strain.

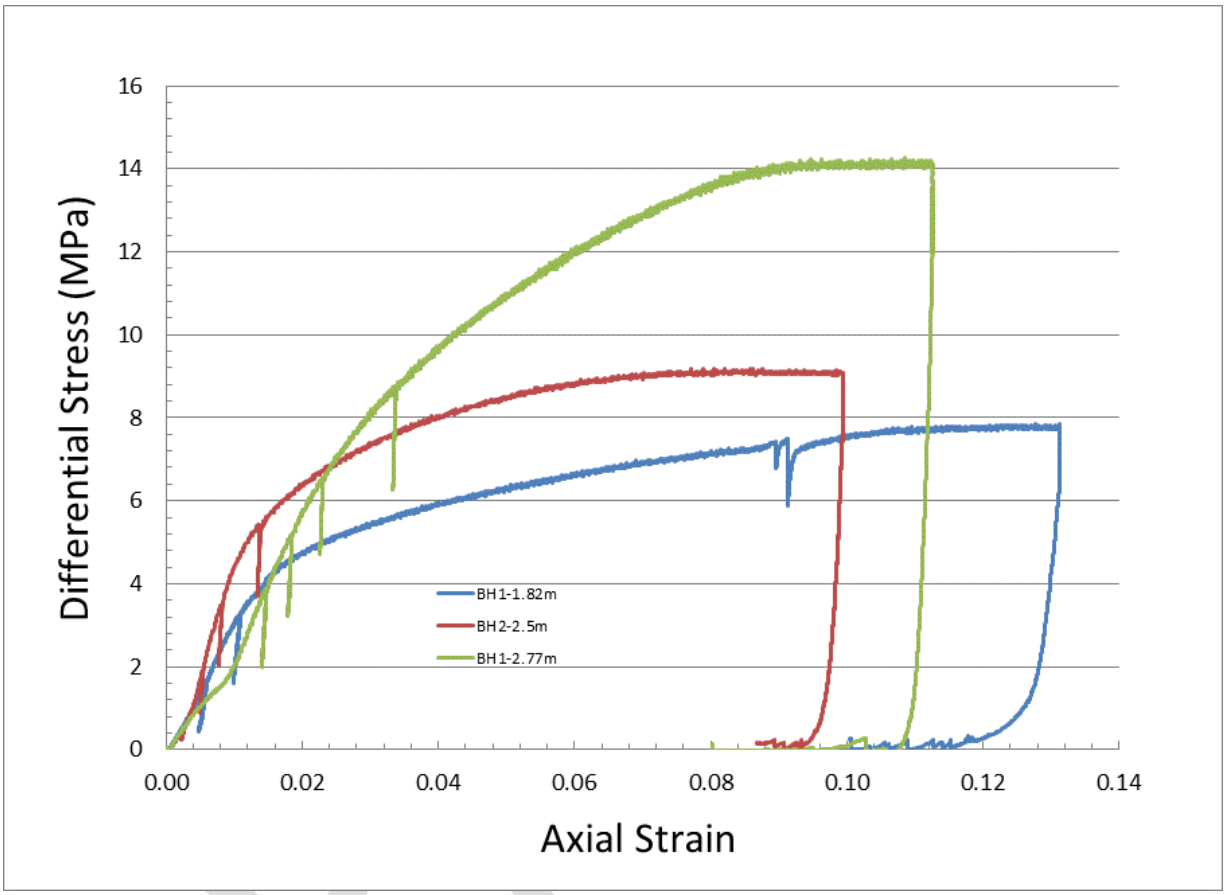

Figure 3.4. Axial stress versus axial strain.

Table 3.2. Modulus calculated at specific axial strains

Sample ID	Confining Pressure (MPa)	E (GPa)	Axial Strain
BH1-1.82m	0.5	1.6	0.0055
		2.5	0.0104
BH2-2.5m	1.0	2.5	0.0144
	1.0	3.2	0.0183
	1.0	4.5	0.023
	1.0	5.5	0.03
BH1-2.77m	0.5	0.7	0.00245
	1.0	1.8	0.00515
	2.07	2.9	0.00795
	2.07	3.7	0.0136

4 CONCLUDING REMARKS

Physical, mechanical, thermal and hydrological measurements have been made on four specimens of reconsolidated salt from the BAMBUS site. A variety of applied procedures and results are documented in this report. This compilation provides independent input to characterization studies undertaken by IfG. Any conclusions on the larger-scale application of the information contained in this report are the prerogative of IfG.

The core for this study derives from emplaced granular material that was subject to compression *in situ* during a long-term experiment. The original backfill was placed at a porosity estimated at 35% and has now consolidated to a variable porosity between 20 and 25%. The variability and magnitude of porosity are consistent among measurement techniques employed in this research. Consolidation was dominated by brittle, mechanical processes with little crystal plasticity and virtually no moisture-aided grain-boundary processes. Permeability to gas was in the range of $5E^{-13}m^2$., decreasing slightly as deformation ensued.

Samples were competent but friable, exhibiting pressure-sensitive strength maxima after 10% axial strain of 8, 9, and 14 MPa at confining pressures of 0.5, 1.0 and 2.0 MPa. Unload/reload moduli increased as a function of deformation. Thermal conductivity increased as porosity decreased and decreased as temperature increased.

5 REFERENCES

Bechthold, W., E. Smailos, S. Heusermann ,W. Bollingerfehr, B. Bazargan Sabet, T. Rothfuchs, P. Kamlot, J. Grupa, S. Olivella, and F. D. Hansen. 2004. *Backfilling and Sealing of Underground Repositories for Radioactive Waste in Salt (BAMBUS II Project*: final report. European Commission. Directorate General for Research. Office for Official Publications of the European Communities. Call No: EUR 20621 EN.

Instruction Manual: Hot Disk thermal Constants Analyzer. Software Version 5.9.

APPENDIX A

The following figures and photographs were provided by IfG for identification of sample origin. Figure A-1 is a plan view of the underground area from whence the new cores were extracted. Notably the coring occurred proximal to the surface of heater 4 as indicated in Figure A-2, Figure A-3, and Figure A-4. Figure A-5, Figure A-6, and Figure A-7 are photographs of the core. Usage of this core is described in the text and summarized in Table 1.1.

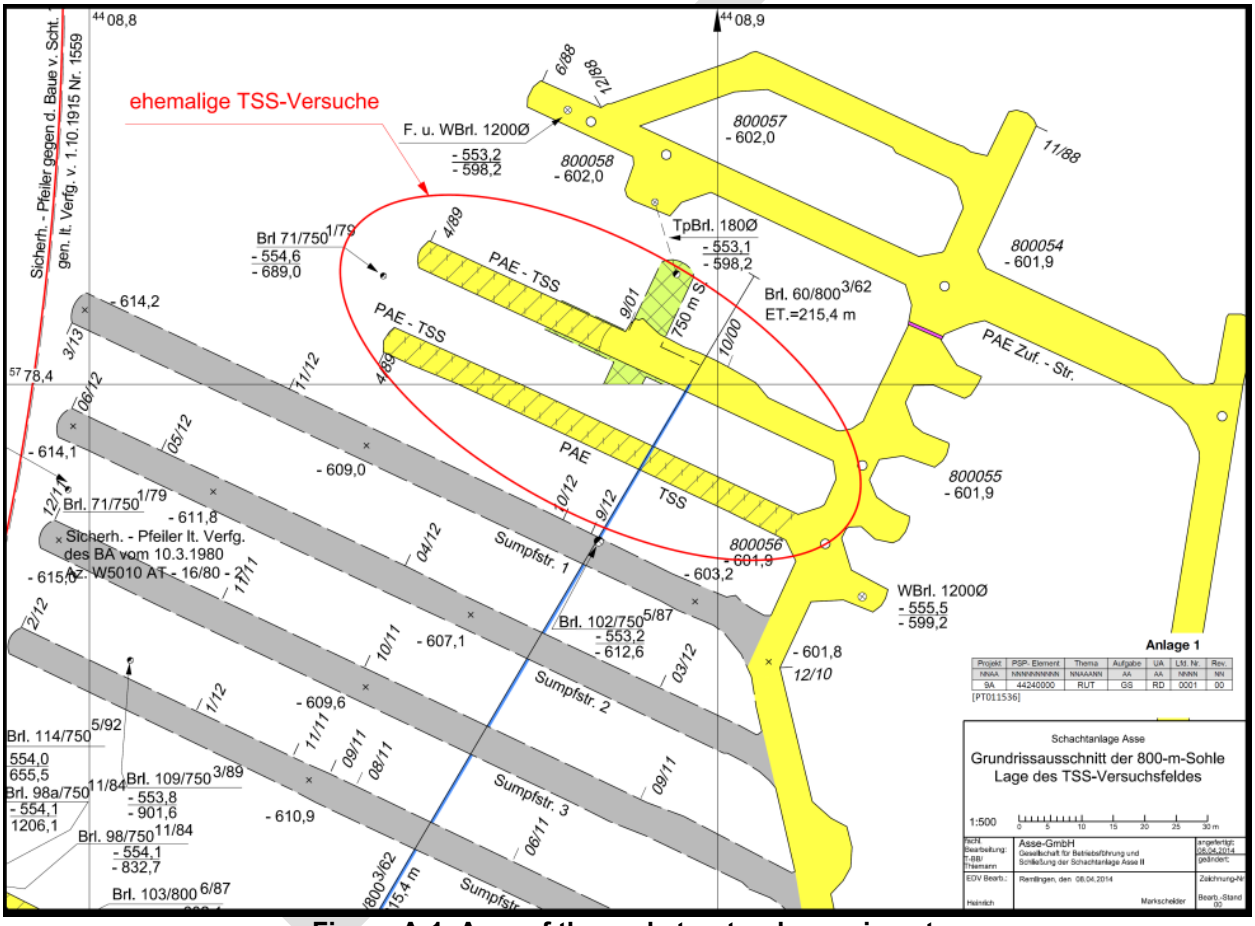

Figure A-1. Area of thermal structural experiment.

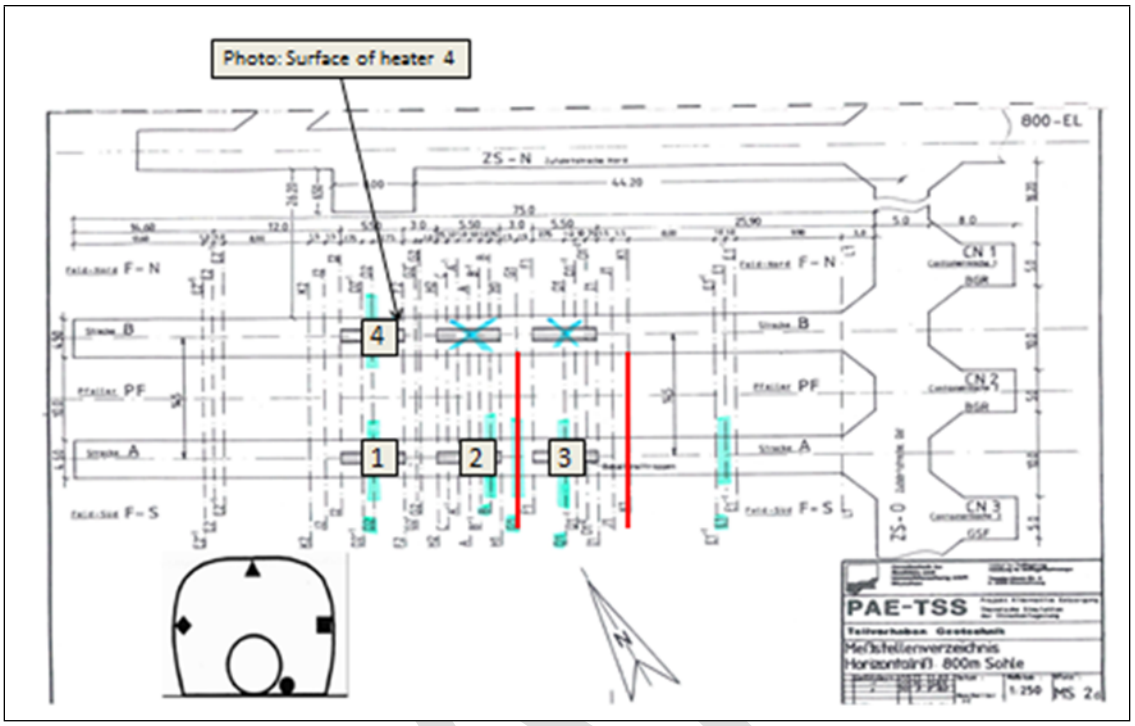

Figure A-2. Plan view of source of new core.

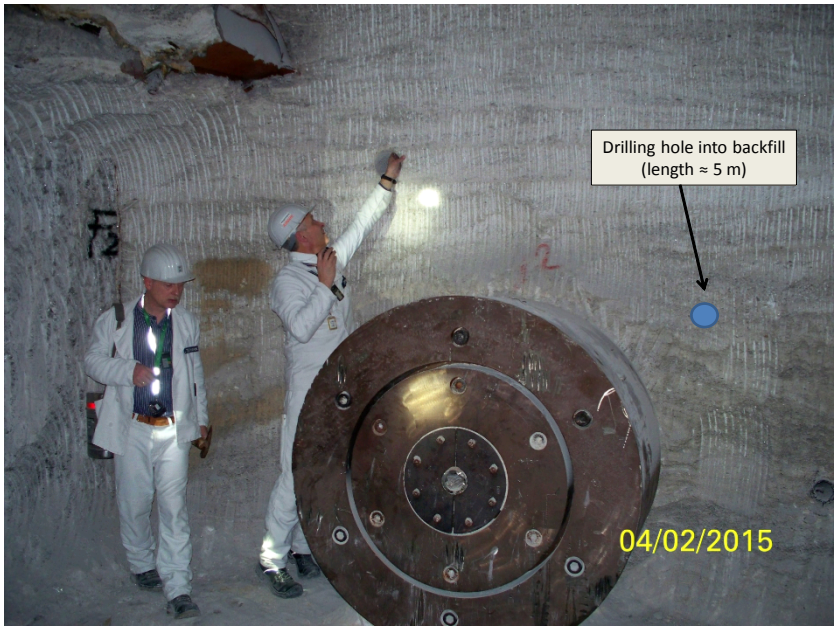

Figure A-3. Surface of heater 4 with man showing borehole Kbrg-1.

Figure A-4. Photographs of Borehole KBrg-2.

Figure A-5. Two samples from KBrg-1 (1.82-2.77m).

Figure A-6. Sample from KBrg-2 (2.5m).

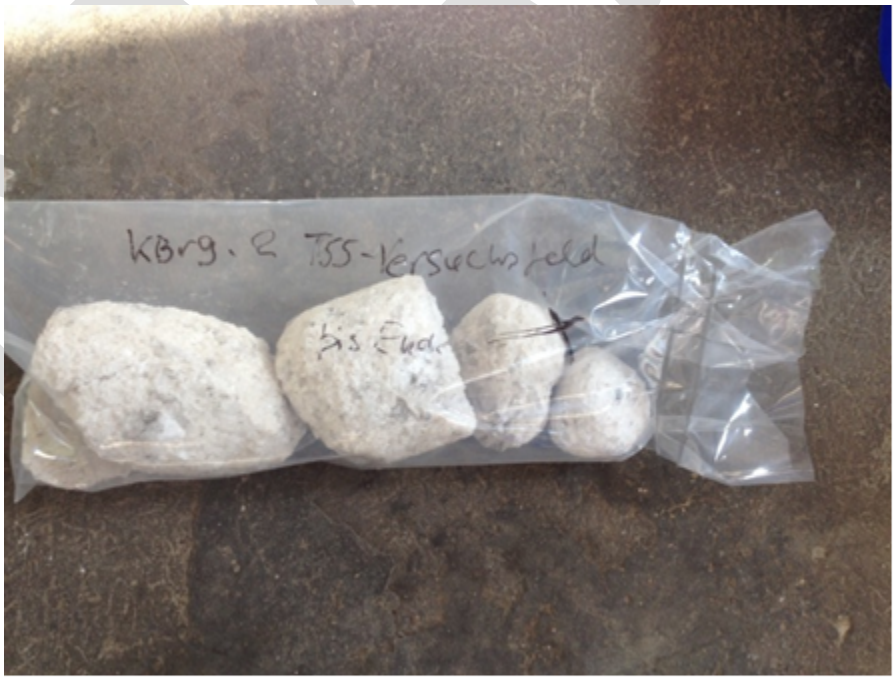

Figure A-7. Sample from KBrg-2 (bis end).

Distribution

2	MS0751	F. D. Hansen	6930
1	MS0779	M. M. Mills	6922
1	MS1033	S.J. Bauer	6914
1	MS1033	S. T. Broome	6914
1	MS1033	P. C. Barrow	6914
1	MS0899	Technical Library	9536 (electronic copy)


Sandia National Laboratories